



Geophysical Research Letters

Supporting Information for

Ozone-induced climate change propped up by the Southern Hemisphere oceanic front

Authors and affiliations

Fumiaki Ogawa, Geophysical Institute, University of Bergen, Bergen, Norway, and Bjerknes Centre for Climate Research, Bergen, Norway.

Nour-Eddine Omrani, Geophysical Institute, University of Bergen, Bergen, Norway,

Bjerknes Centre for Climate Research, Bergen, Norway, and Helmholtz Centre for Ocean Research Kiel (GEOMAR), Kiel, Germany.

Kazuaki Nishii, Research Center for Advanced Science and Technology, University of Tokyo, Tokyo, Japan.

Hisashi Nakamura, Research Center for Advanced Science and Technology, University of Tokyo, Tokyo, Japan, and Japan Agency for Marine-Earth Science and Technology, Yokohama, Japan

Noel Keenlyside, Geophysical Institute, University of Bergen, Bergen, Norway, and Bjerknes Centre for Climate Research, Bergen, Norway.

Corresponding author: F. Ogawa, Geophysical Institute, University of Bergen, Bergen, Norway.

Allégaten 70, Bergen, 5007, Norway. (fumiaki.ogawa@gfi.uib.no)

Contents of this file

Text S1
Figures S1 to S11
Tables S1 to S2

Introduction

This supporting information is prepared to describe the analysis methods more in detail (text S1) and more evidences (Figures S1 to S11 and Tables S1 to S2) to support our arguments in the main text but is not necessarily required to show in the main text.

Text S1. Methods

1.1. Experimental design of the prescribed sea-surface temperature

Following the previous studies [Nakamura et al., 2008; Sampe et al., 2013], we linearly interpolated SST from the poleward flank (at 53°S) of the oceanic front toward the South Pole (black solid lines in Figures 2a-b), where SST is set to 0°C and sea-ice is assumed to be absent. As in the previous studies [Nakamura et al., 2008; Sampe et al., 2013], the frontal SST gradient was eliminated for the “non-front experiments” by interpolating SST from the equatorward flank (at 40°S) of the front to the pole (green dashed lines in Figures 2a-b). This procedure introduces artificial warming over the subpolar ocean and thus artificially enhances heat and moisture release into the atmosphere, which can enhance moist diabatic growth of storms. In the non-front experiments, both the climatological storm-track activity and eddy-driven midlatitude westerlies nevertheless weaken substantially (Fig. S2), indicative of the importance of the frontal SST gradient for shaping the climatological-mean atmospheric circulation in the extratropics. Importantly, the particular procedure yields no change in subtropical SST. Otherwise, the atmospheric meridional overturning circulation in the Tropics (Hadley cell) and the associated subtropical westerly jetstream would change, giving rise to substantial modifications in the midlatitude westerlies and storm-track activity and thus making it difficult to isolate the impacts of the midlatitude SST gradients. For all the experiments the SST profile in the Tropics and the model Northern Hemisphere (NH) is kept the same, and the profile in the model SH used for the non-front experiments was prescribed in the model NH after imposing the lag of 6 months.

1.2. Definition of stratospheric year-to-year variability

The contribution of the leading mode to the total variance of the 13-hPa westerly variability is 80.1 (83.3) % when the steep midlatitude SST gradient (oceanic front) is present (absent). Since the meridional structure of the leading mode of the stratospheric year-to-year variability in our experiments is rather insensitive to the ozone profile (Figures S9a-b), we combined the outputs from the two experiments with and without the ozone depletion under the same SST profiles for our EOF analysis that was utilized for constructing Figures 3c-d.

1.3. Procedure for SAM time-scale analysis

The definition of “decorrelation time-scale” referred in this paper to evaluate the SAM persistency is basically identical to the one discussed in Baldwin et al. (2003). After low-pass filtering (31 day running mean) is performed on daily time-series of zonal mean zonal wind, its daily climatology (seasonal cycle) is subtracted. We then apply EOF analysis on the daily anomaly time series separately for each pressure level between 20°S to the South Pole. Then auto-correlation analysis is applied on the year-to-year anomaly of PC1 time series for each pressure level and day of year. The decorrelation time-scale is then calculated as the e-folding lag (days) of the autocorrelation coefficient.

1.4. Analyses procedure of CMIP models

Both CMIP3 and CMIP5 were led by the World Climate Research Programme's Working Group on Coupled Modelling [Meehl et al., 2007; Taylor et al., 2012]. Outputs from the climate models are available at the web site of the Program for Climate Model Diagnosis and Intercomparison (PCMDI). We focus on particular experiments called “20th century climate in coupled model (20C3M)” and “HISTORICAL” for the CMIP3 and CMIP5 models, respectively, both of which aim to simulate the 20th century climate. Refer to <http://cmip-pcmdi.llnl.gov/index.html> for more details. The climatology and trend of the westerlies and oceanic fronts were calculated for austral summer (Dec-Feb) over 20 years from 1979/80 to 1998/99, while those of stratospheric (100 hPa) temperature over Antarctica (poleward of 70°S) were calculated for spring and early summer (Oct-Jan). The climatological latitude of the oceanic front in the midlatitude SH in a given model was identified first by finding the peak latitude of the meridional gradient of zonal-mean SST between 30°S and 55°S in each year and then averaging it over the entire 20-year period. When averaged zonally, none of the SST fields used in JRA-25 and 67 out of those 73 CMIP3/5 models exhibits any apparent poleward shift of the SST front during the late 20th century.

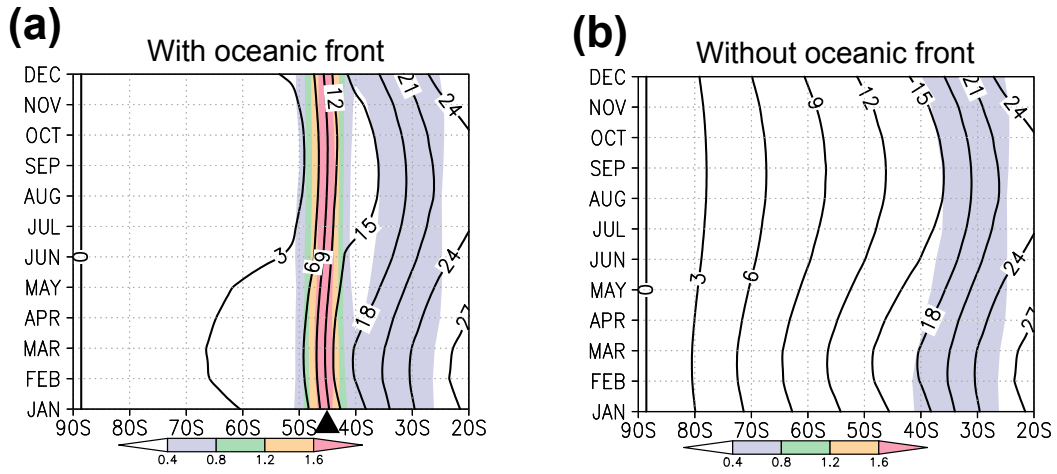


Figure S1. Latitude-time sections showing the seasonal march of zonally symmetric SST prescribed for the AGCM experiments. Contours indicate SST ($^{\circ}\text{C}$) and shading indicates its meridional gradient ($^{\circ}\text{C}/\text{latitude}$) for the experiments (a) with and (b) without the oceanic front.

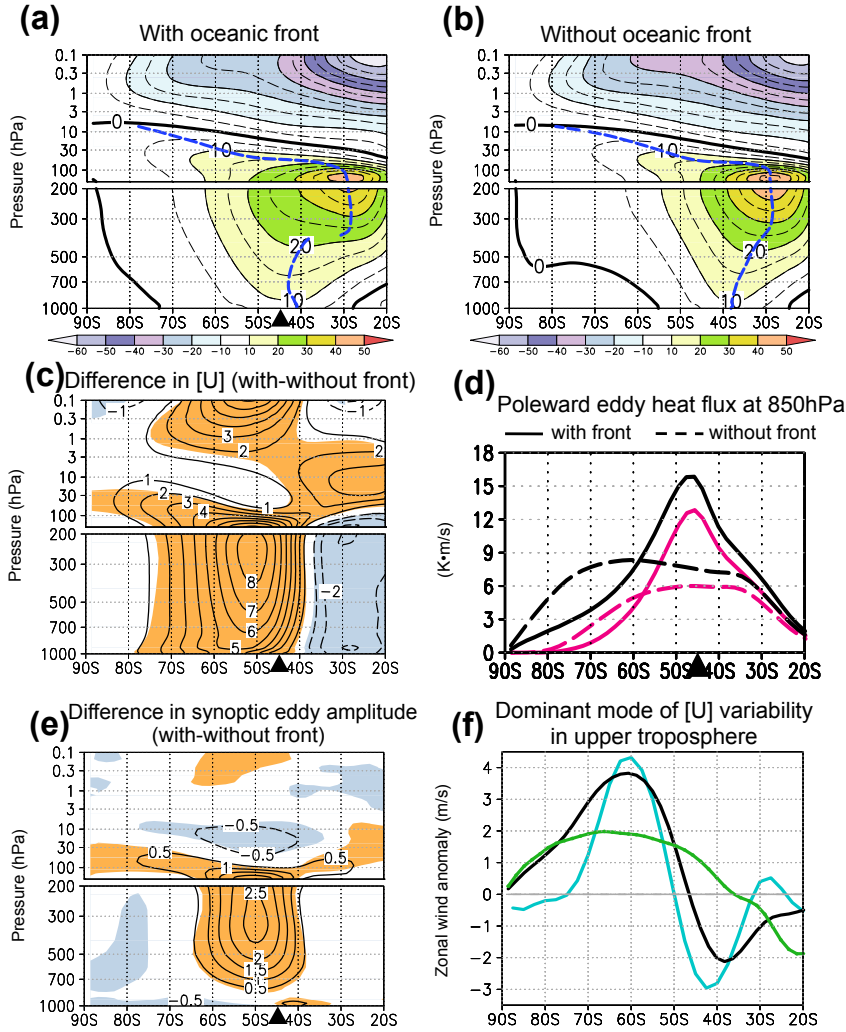


Figure S2. Climatological zonal-mean westerlies and lower-tropospheric eddy heat flux averaged between 16th November and 16th December. (a) Meridional section of climatological westerlies averaged over both the high- and low-ozone experiments with the oceanic front. Intervals are 10ms^{-1} and 5ms^{-1} for thin-solid and thin-dashed lines, respectively. Thick solid lines indicate zero wind speed. Blue dashed lines indicate the climatological westerly axes. Black triangle indicates the latitude of the oceanic front. (b) As in (a), but for the experiments without the front. (c) Difference between (a) and (b). Shading indicates the response exceeding the 5% significance based on the Student's t-test. (d) Latitudinal profiles of climatological-mean 850hPa poleward eddy heat fluxes, evaluated from local deviations in temperature and meridional wind velocity from their zonal means (black) and only from synoptic-scale eddies (zonal wavenumbers 4 and above, red), for the experiments with (solid) and without (dashed) the front. (e) As in (c), but for the difference in the standard deviation of meridional wind fluctuations associated with the synoptic-scale eddies. (f) As in (d), but for 31-day running means of 276-hPa zonal-mean zonal wind anomalies regressed on the standardized PC1 time series of its year-to-year variability simulated in the presence (black) and absence (green) of the oceanic front. The observational counterpart as 300-hPa zonal-mean zonal wind anomaly in December (1979-2013) based on the JRA-25 reanalysis is superimposed (blue).

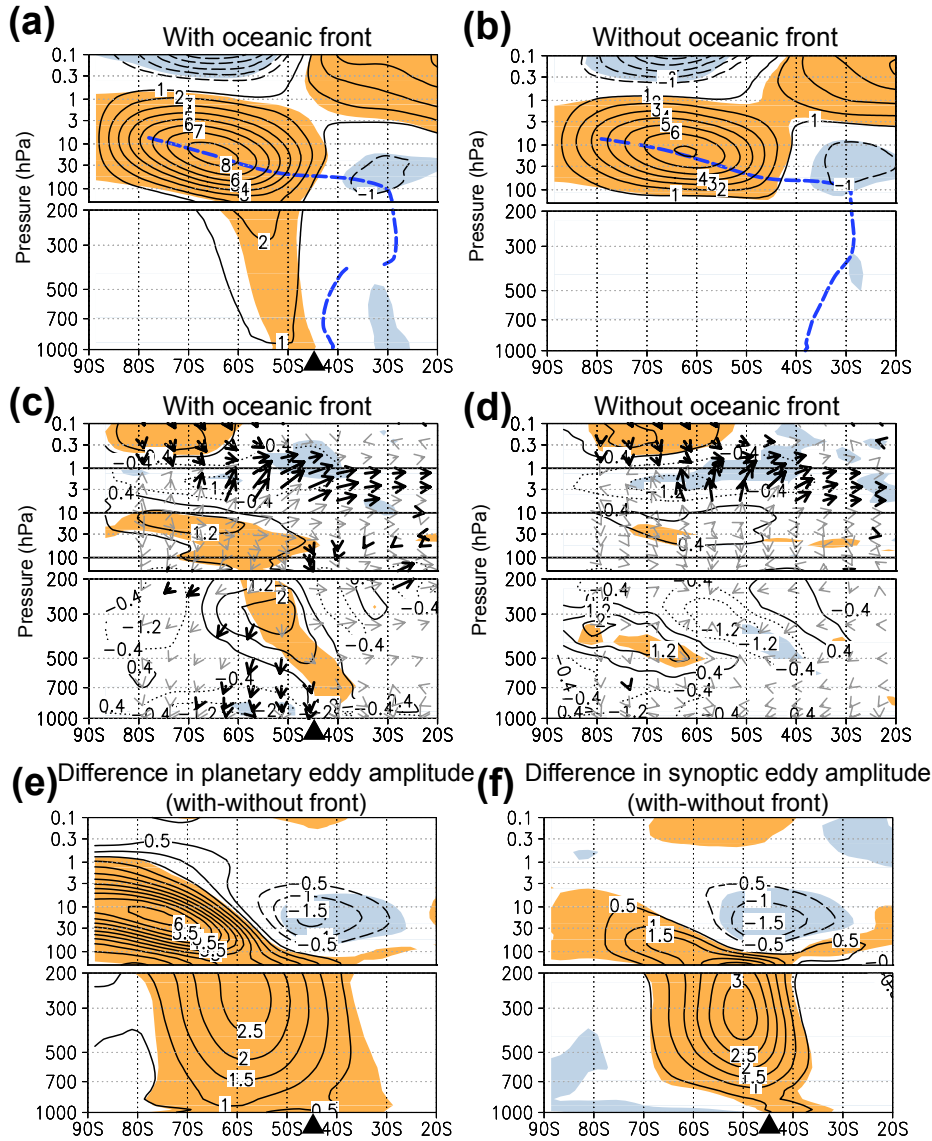


Figure S3. Meridional sections showing the structure of the early-summer atmospheric response simulated to the prescribed ozone depletion. (a)-(b) Zonal-mean zonal wind response in the 31-day average from 16th November to 16th December (contoured for every 1 m s^{-1} ; solid and dashed lines for anomalous westerlies and easterlies, respectively) for experiments (a) with and (b) without the oceanic front. Shading indicates the response exceeding the 5% statistical significance based on the Student's t-test. Dashed lines denote the climatological axes of the westerlies. Black triangle indicates the latitude of the oceanic front. (c)-(d) As in (a)-(b), respectively, but for anomalous EP flux (vector, darker for 5% significance) and westerly forcing estimated by its divergence ($\text{m s}^{-1}/\text{day}$; contour) as the 7-day average from 10th to 16th November. (e)-(f) As in (a)-(b), respectively, but for anomalous standard deviation of eddy meridional wind fluctuations associated with the (e) planetary-scale and (f) synoptic-scale waves.

With oceanic front

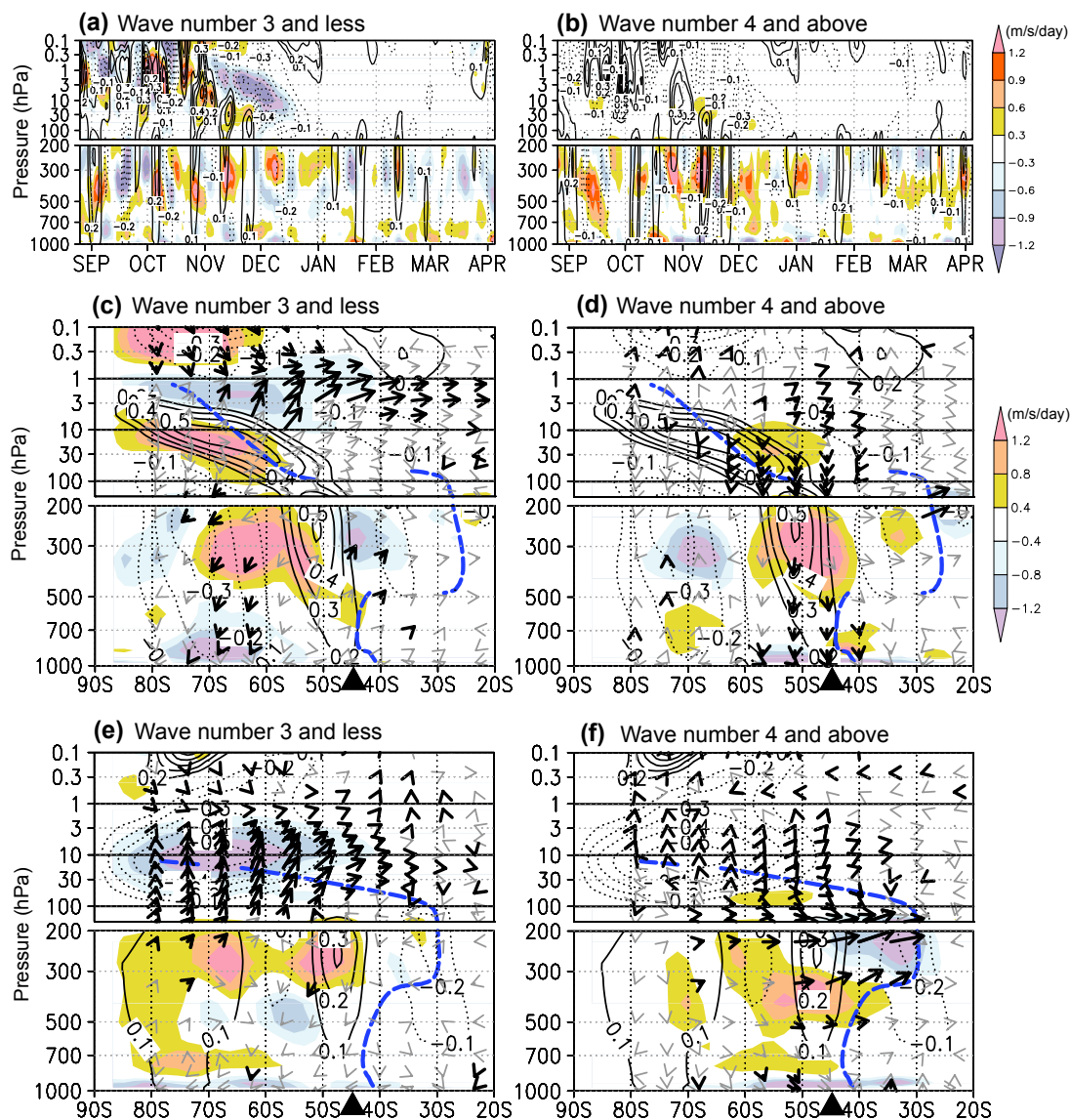


Figure S4. Eddy forcing of the westerly mean-flow in the period of tropospheric westerly response to the ozone depletion in the presence of the oceanic front. (a)-(b) Time-height sections of the westerly tendency ($\text{m s}^{-1}/\text{day}$; contour) and EP-flux divergence ($\text{m s}^{-1}/\text{day}$; shade) associated with the (a) planetary and (b) synoptic-scale waves, averaged between (a) 50°S and 70°S and (b) 45°S and 60°S , respectively. (c)-(d) Anomalous EP flux (vector, darker for the 5% significance), westerly forcing estimated by its divergence ($\text{m s}^{-1}/\text{day}^{-1}$; shade) and simulated westerly tendency ($\text{m s}^{-1}/\text{day}$; contour), as the 7-day averages from the 10th to 16th of November, in association with the (c) planetary and (d) synoptic-scale waves. (e)-(f) As in (c)-(d), respectively, but for the 7-day averages from the 3rd to 9th of December.

Without oceanic front

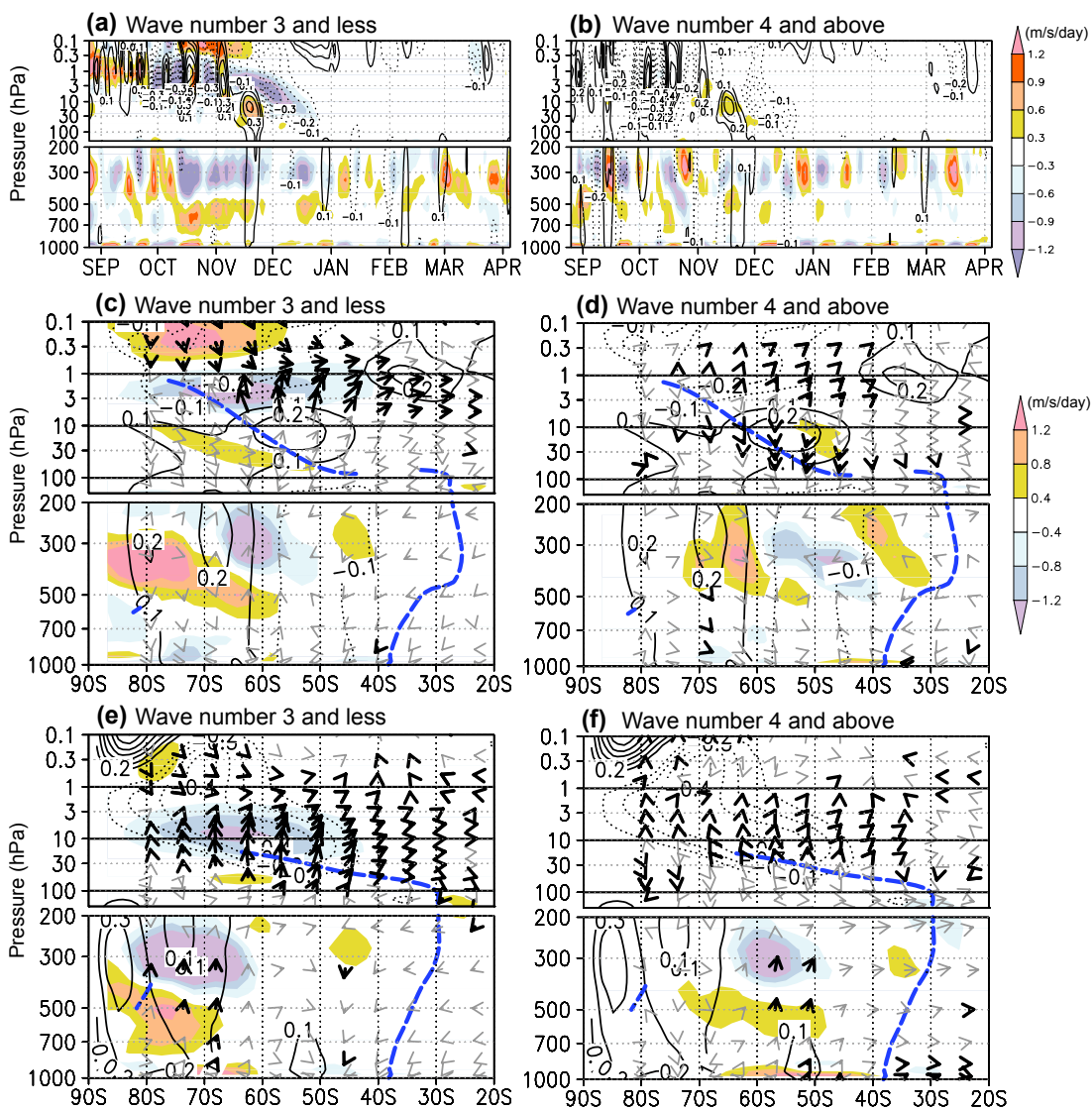


Figure S5. Same as in Figure S4, but for the absence of the oceanic front.

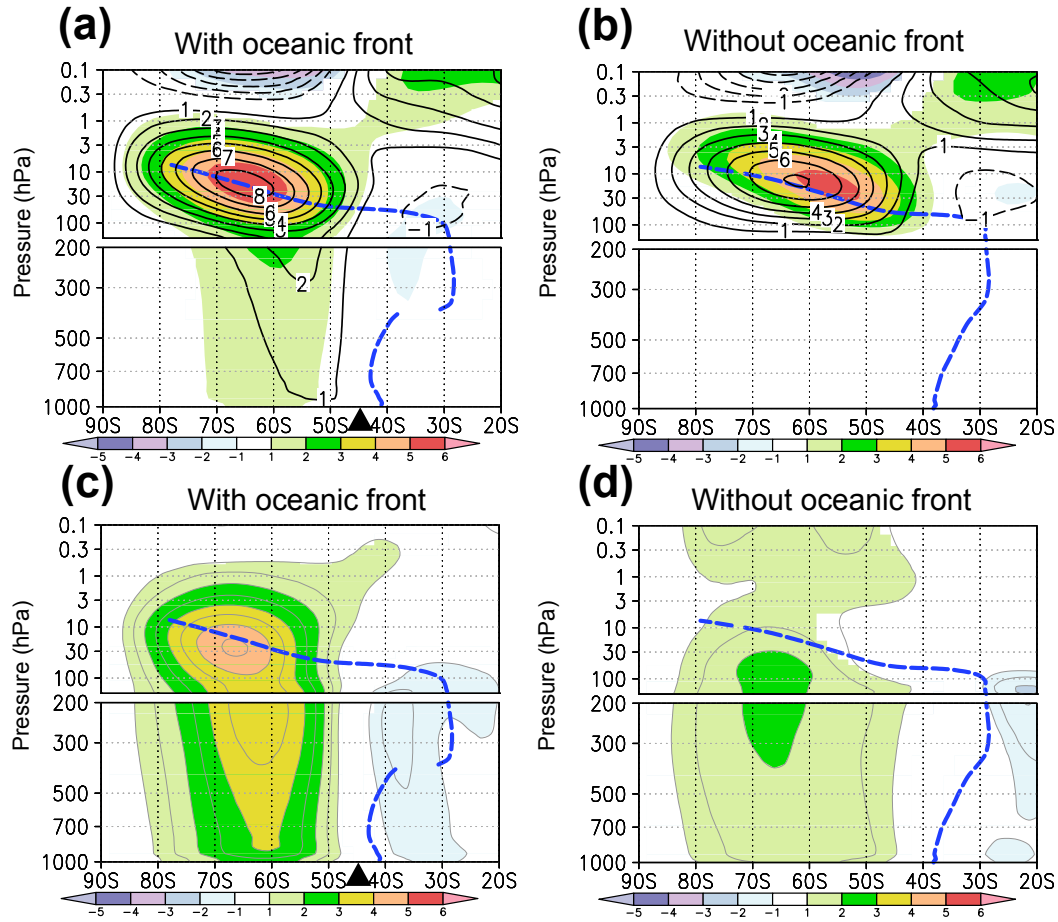


Figure S6. Meridional sections showing the westerly response to the ozone depletion and anomalous westerlies associated with the year-to-year SAM variability. (a)-(b) Ozone-induced changes in zonal-mean westerlies (contoured as in Fig. 3a), and anomalous westerlies (color shaded) associated with the stratospheric SAM variability, both averaged over 31 days between 16th November and 16th December, as simulated in experiments (a) with the oceanic front and (b) without it. The shaded anomalies, obtained by regressing westerly anomalies linearly on the PC1 time series defined at 13hPa on 15th November, correspond to the year-to-year anomalies for the PC1 value of a unit standard deviation. Only the anomalies that are significant at the 5% level are shaded. Dashed lines denote the climatological axes of the westerlies. (c)-(d) Tropospheric SAM signature as estimated by regressing the zonal-mean anomalous westerlies on PC1 for the 857hPa zonal-mean wind anomalies on 1st December (shading), both averaged over 31 days between 16th November and 16th December, as simulated in experiments (c) with and (d) without the oceanic front. The signature is also indicated by gray contours with the interval of $0.5 \text{ (m s}^{-1}\text{)}$.

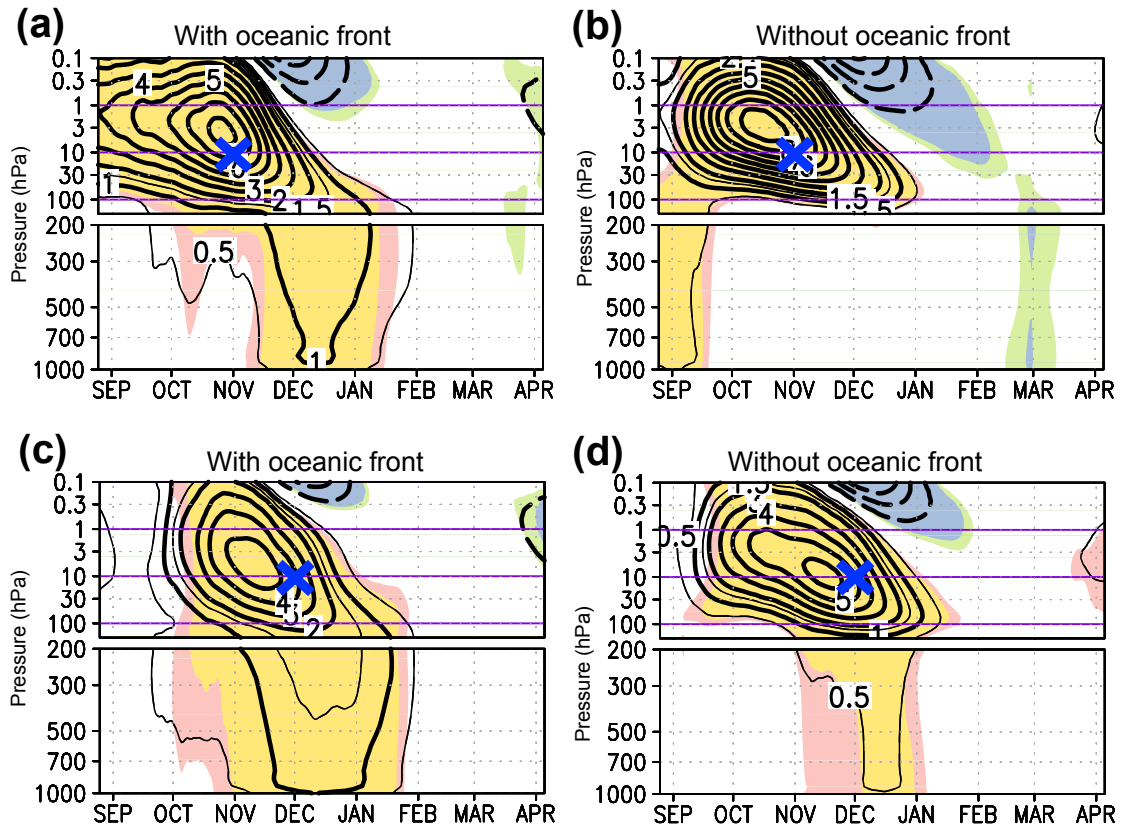


Figure S7. Same as in Figures 3c-d, but for different reference dates for the stratospheric anomalies. (a)-(b) 1st November. (c)-(d) 1st December. Signals significant at the 5 (1)% level estimated from the correlation coefficient are colored pink (yellow) for westerly anomalies and green (blue) for easterly anomalies.

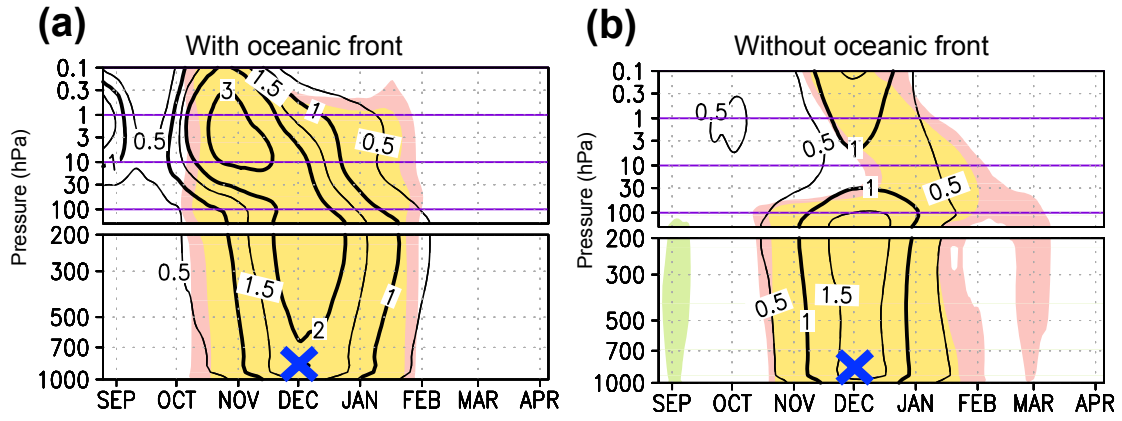


Figure S8. Same as in Figures 3c-d, but for the reference pressure level at 857hPa.

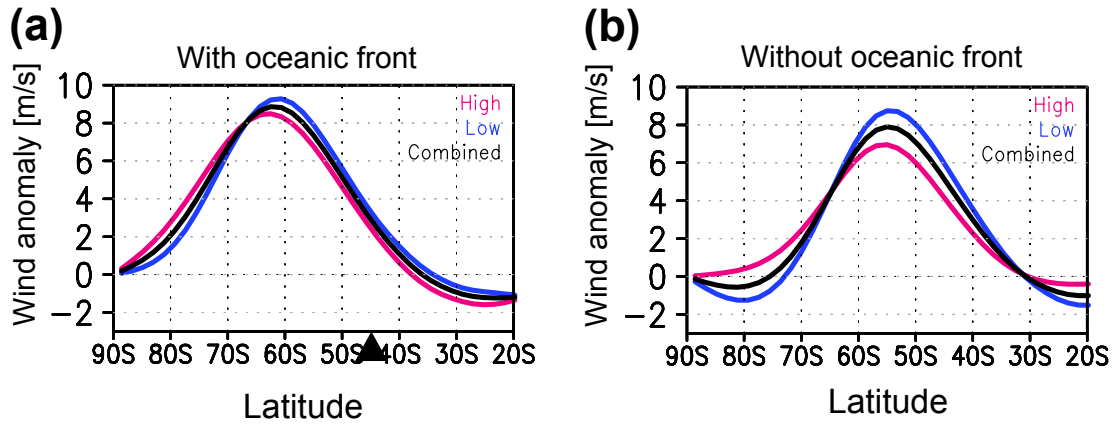


Figure S9. Latitudinal profiles showing the 31 day-running mean anomalies of 13hPa zonal wind on 15th November associated with the dominant mode of stratospheric year-to-year variability (EOF1, see methods for details) in experiments (a) with and (b) without the oceanic front. Red (blue) lines indicate the profiles for the experiments where the prescribed ozone concentration is higher (lower). Black lines indicate the profiles based on the combined time series over both the high- and low-ozone experiments.

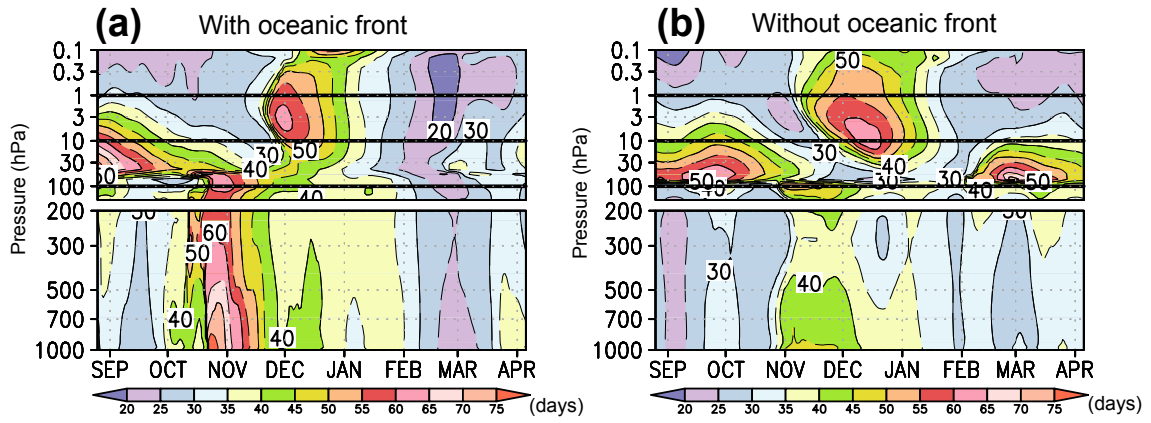


Figure S10. Seasonality of the decorrelation time-scale (in days) of the simulated annular mode signature (see supplementary texts S1-3 for details) at each pressure level simulated (a) with and (b) without the oceanic front.

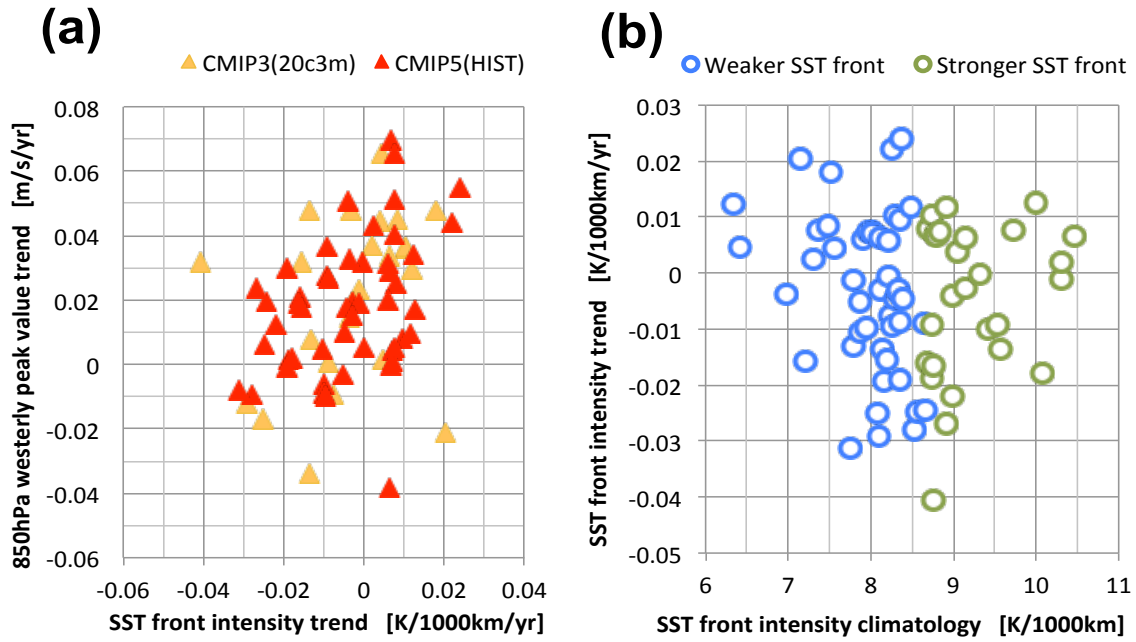


Figure S11. Relationships between midlatitude zonal-mean statistics among the CMIP3/5 models (orange/red triangles, respectively). (a) Between linear trends in maximum speed of 850hPa westerlies and in SST front intensity. (b) Between climatological intensity and linear trend of SST front. In (b), blue (green) symbols indicate models with weaker (stronger) mean SST front compared to the JRA-25 reanalysis data.

Model name	Ocean front	Temp. trend	Atmos. grid	Institution(s)
BCCR-BCM2.0	S	NSC	128x64	Bjerknes Centre for Climate Research
CGCM3.1(T47)	W	W	96x48	Canadian Centre for Climate Modelling & Analysis
CGCM3.1(T63)	W	NSC	128x64	
CNRM-CM3	W	NSC	128x64	Météo-France / Centre National de Recherches Météorologiques
CSIRO-Mk3.0	W	SC	192x96	CSIRO Atmospheric Research
CSIRO-Mk3.5	S	SC	192x96	
GFDL-CM2.0	W	W	144x90	US Dept. of Commerce / NOAA / Geophysical Fluid Dynamics Laboratory
GFDL-CM2.1	W	SC	144x90	
GISS-AOM	W	NSC	90x60	NASA / Goddard Institute for Space Studies
GISS-EH	W	NSC	72x45	
GISS-ER	W	SC	72x45	
FGOALS-g1.0	W	SC	128x60	LASG / Institute of Atmospheric Physics
INGV-SXG	W	SC	320x160	Instituto Nazionale di Geofisica e Vulcanologia
INM-CM3.0	W	W	72x45	Institute for Numerical Mathematics
IPSL-CM4	S	NSC	96x72	Institut Pierre Simon Laplace
MIROC3.2(hires)	W	NSC	320x160	Center for Climate System Research (The University of Tokyo), National Institute for Environmental Studies, and Frontier Research Center for Global Change (JAMSTEC)
MIROC3.2(medres)	S	SC	128x64	
ECHAM5/MPI-OM	W	NSC	192x96	Max Planck Institute for Meteorology
MRI-CGCM2.3.2	W	NSC	128x64	Meteorological Research Institute
CCSM3	S	SC	256x128	National Center for Atmospheric Research
PCM	S	SC	128x64	
UKMO-HadCM3	S	SC	96x73	Hadley Centre for Climate Prediction and Research / Met Office
UKMO-HadGEM1	S	NSC	192x145	

Table S1. List of the 23 CMIP3 models used in the present study. In the second column, “S” and “W” indicate that the SH oceanic front simulated in a particular model is stronger or weaker, respectively, compared to the SST field used for JRA-25. In the third column, “SC” and “NSC” indicate that a cooling trend simulated in the stratosphere (100-hPa) over Antarctica from 1979/80 to 1998/99 in austral spring/summer (Oct–Jan) exceeds the 1% significance level or not, respectively, and “W” indicates that the simulated trend is warming rather than cooling. The fourth column denotes the numbers of grid points in longitude and latitude for atmospheric data provided.

Model name	Ocean front	Temp. trend	Atmos. grid	Institution(s)
ACCESS1-0	W	SC	192x145	CSIRO (Commonwealth Scientific and Industrial Research Organisation, Australia), and BOM (Bureau of Meteorology, Australia)
ACCESS1-3	W	NSC	192x145	
BCC-CSM1.1	S	SC	128x64	Beijing Climate Center, China Meteorological Administration
BCC-CSM1.1(m)	S	NSC	320x160	
BNU-ESM	S	NSC	128x64	College of Global Change and Earth System Science, Beijing Normal University
CanCM4	S	NSC	192x96	Canadian Centre for Climate Modelling and Analysis
CanESM2	S	SC	192x96	
CCSM4	S	SC	288x192	National Center for Atmospheric Research
CESM1-BGC	S	NSC	288x192	National Science Foundation, Department of Energy, National Center for Atmospheric Research
CESM1-CAM5	W	NSC	288x192	
CESM1-FASTCHEM	S	SC	288x192	
CESM1-WACCM	W	SC	144x96	
CMCC-CESM	W	NSC	96x48	Centro Euro-Mediterraneo per I Cambiamenti Climatici
CMCC-CM	W	SC	480x240	
CMCC-CMS	S	NSC	192x96	
CNRM-CM5	W	NSC	256x128	Centre National de Recherches Météorologiques / Centre Européen de Recherche et Formation Avancées en Calcul Scientifique
CNRM-CM5.2	W	NSC	256x128	
CSIRO-Mk3.6.0	S	NSC	192x96	Commonwealth Scientific and Industrial Research Organisation in collaboration with the Queensland Climate Change Centre of Excellence
CSIRO-Mk3L-1.2	W	W	64x56	
EC-EARTH	W	NSC	320x160	EC-Earth consortium
FGOALS-g2	W	SC	128x60	LASG, Institute of Atmospheric Physics, Chinese Academy of Sciences
FGOALS-s2	S	NSC	128x108	
FIO-ESM	W	NSC	128x64	The First Institute of Oceanography, SOA, China
GFDL-CM2.1	W	NSC	144x90	Geophysical Fluid Dynamics Laboratory
GFDL-CM3	W	SC	144x90	
GFDL-ESM2G	W	SC	144x90	
GFDL-ESM2M	W	SC	144x90	
GISS-E2-H	W	SC	144x90	NASA Goddard Institute for Space Studies
GISS-E2-H-CC	W	SC	144x90	
GISS-E2-R	W	SC	144x90	
GISS-E2-R-CC	W	SC	144x90	

Table S2. As in Table S1 but for the 50 CMIP5 models.

Model name	Ocean front	Temp. trend	Atmos. grid	Institution(s)
HadCM3	S	NSC	96x73	Met Office Hadley Centre
HadGEM2-AO	W	NSC	192x145	National Institute of Meteorological Research/Korea Meteorological Administration
HadGEM2-CC	W	NSC	192x145	Met Office Hadley Centre
HadGEM2-ES	W	NSC	192x145	
INMCM4	W	SC	180x120	Institute for Numerical Mathematics
IPSL-CM5A-LR	S	SC	96x96	Institut Pierre-Simon Laplace
IPSL-CM5A-MR	S	NSC	144x143	
IPSL-CM5B-LR	W	SC	96x96	
MIROC4h	W	SC	640x320	Atmosphere and Ocean Research Institute (The University of Tokyo), National Institute for Environmental Studies, and Japan Agency for Marine-Earth Science and Technology
MIROC5	W	SC	256x128	
MIROC-ESM	S	NSC	128x64	Japan Agency for Marine-Earth Science and Technology, Atmosphere and Ocean Research Institute (The University of Tokyo), and National Institute for Environmental Studies
MIROC-ESM-CHEM	S	SC	128x64	
MPI-ESM-LR	W	NSC	192x96	Max Planck Institute for Meteorology (MPI-M)
MPI-ESM-MR	S	NSC	192x96	
MPI-ESM-P	W	SC	192x96	
MRI-CGCM3	W	NSC	320x160	Meteorological Research Institute
MRI-ESM1	W	NSC	320x160	
NorESM1-M	S	NSC	144x96	Norwegian Climate Centre
NorESM1-ME	S	SC	144x96	

Table S2. Continued.

References

- Nakamura, H., T. Sampe, A. Goto, W. Ohfuchi, and S.-P. Xie (2008), On the importance of midlatitude oceanic frontal zones for the mean state and dominant variability in the tropospheric circulation, *Geophys. Res. Lett.*, *35*, L15709, doi: 10.1029/2008GL034010.
- Sampe, T., H. Nakamura and A. Goto (2013), Potential influence of a midlatitude oceanic frontal zone on the annular variability in the extratropical atmosphere as revealed by aqua-planet experiments. *J. Meteorol. Soc. Jpn.*, *91a*, 243–267, doi: 10.2151/jmsj.2013-A09.
- Meehl, G. A. *et al.* (2007), The WCRP CMIP3 multi-model dataset: A new era in climate change research, *Bull. Am. Meteorol. Soc.*, *88*, 1383–1394, doi: 10.1175/BAMS-88-9-1383.
- Taylor, K. E., R. J. Stouffer, and G. A. Meehl (2012), An overview of CMIP5 and the experiment design, *Bull. Am. Meteorol. Soc.*, *93*, 485–498, doi: 10.1175/BAMS-D-11-00094.1.